International Symposium
On Turbulence and Shear Flow
Phenomena (TSFP-9)
June 30 - July 3, 2015 *Melbourne, Australia*

LARGE EDDY SIMULATION OF CRYOGENIC COAXIAL LN2/GH2 INJECTION UNDER SUPERCRITICAL PRESSURES

Jan Matheis[1]*, Hagen Müller[2], Michael Pfitzner[2] and Stefan Hickel[1,3]
1: Institute of Aerodynamics and Fluid Mechanics, Technische Universität München, Germany.
2: Institute for Thermodynamics, Universität der Bundeswehr München, Germany.
3: Aerodynamics Group, Faculty of Aerospace Engineering, Technische Universiteit Delft, The Netherlands.
*Corresponding author: jan.matheis@tum.de

ABSTRACT

The coaxial injection of cryogenic nitrogen and warm hydrogen into a supercritical nitrogen atmosphere is studied numerically by means of well resolved large-eddy simulation (LES). Numerical data for two operating conditions are compared both quantitatively and qualitatively with a series of experiments [Oschwald et al., 35th AIAA/ASME/SAE/ASEE Joint Propulsion Conference, 1999]. A detailed thermodynamic analysis of phenomena associated with the binary mixing of nitrogen and hydrogen together with a systematic study of the thermodynamic state of cryogenic nitrogen prior to injection allows an assessment of uncertainties related to both numerical and experimental data. Trans- and supercritical mixing constitutes considerable challenges for numerical simulations with regard to physical modeling and numerical stability. We compare a fully conservative (FC) formulation to a quasi conservative (QC) formulation of the governing equation, which was recently proposed by Terashima and Koshi [J. Comput. Phys., 2012].

INTRODUCTION

Modern high performance Liquid Rocket Engines (LRE) like the Vulcain II engine operate at combustion pressures ($p > 10$ MPa) well above the critical pressures of the injected propellants. Furthermore, operating conditions of most main stage LREs are designed such that one or both propellants enter the thrust chamber at cryogenic temperatures. Hence, the injected propellant is in a transcritical state, characterized by high liquid-like densities and viscosities. In this transcritical regime the physical properties, e.g., density, viscosity and specific heats, are strong non-linear functions of the local pressure and temperature. Therefore, trans- and supercritical mixing constitutes considerable challenges for numerical simulations with regard to physical modeling, numerical stability and computational efficiency. In this context, Terashima & Koshi (2012) recently presented a numerical approach, specifically designed for cryogenic mixing under supercritical pressures, for which the total energy conservation equation is replaced by a pressure evolution equation (PEVO). Their generalized formulation of this equation, valid for complex viscous fluids, has a sort of beauty as it satisfies velocity and pressure equilibrium at fluid interfaces. The motivation to use a PEVO comes from the observation that a fully conservative (FC) formulation together with insufficient grid resolutions may lead to spurious pressure oscillations which deteriorate not only computational stability but also the accurate prediction of flow fields such as turbulence and acoustics (Terashima & Koshi, 2012). For a thorough discussion on the origin of spurious pressure oscillations caused by EOS's peculiarities it is referred to Terashima & Koshi (2012). However, sorting out the total energy conservation equation gives rise to the question: What are the consequences of a poor energy conservation property? Terashima & Koshi (2012) addressed this issue only for one-dimensional single-species advection test cases. Given a lack of robustness of their FC method, no direct comparison between FC and QC formulation was possible for a two-dimensional test case. Following up on this, the objective of this paper is to identify differences between a FC and a QC formulation, with particular emphasis on the energy conservation issue and the thermodynamic consequences, in its application to a realistic three-dimensional test setup. In this context we confine our study to two selected operating conditions of a series of experiments of Oschwald *et al.* (1999) in which quantitative density measurements in a coaxial LN_2/GH_2 jet at supercritical pressures (with respect to the critical pressure of the pure nitrogen) were obtained. This setup is highly challenging both numerically (density ratios between main nitrogen and annular hydrogen jet ranging from 43 to 166) and thermodynamically (real gas mixing effects). In general, shear coaxial injectors, as considered in this work, have been investigated in a number of experiments (see e.g. Mayer *et al.*, 1998; Oschwald *et al.*, 1999; Chehroudi *et al.*, 2002) and numerical simulations (see e.g. Masquelet *et al.*, 2012; Terashima & Koshi, 2014; Müller *et al.*, 2015), thus, there is a qualitative understanding of the underlying physics associated with trans- and supercritical injection and mixing. However, it is worth mentioning that especially quantitative comparisons between experimental data and high-fidelity numerical simulations are scarce. In this context the present work highlights some physical aspects that are associated with trans- and supercritical coaxial injection of LN_2/GH_2.

SETUP AND FLOW CONFIGURATION

Numerical Model for Large Eddy Simulation

We solve the three-dimensional compressible multicomponent Navier-Stokes equations either in a FC formulation, Eq. (1)-(4), or in a QC formulation for which the total energy conservation, Eq. (4), is substituted by a pressure evolution equation, Eq. (5), that can be derived from the total pressure derivative using Eq. (1)-(4). The state vec-

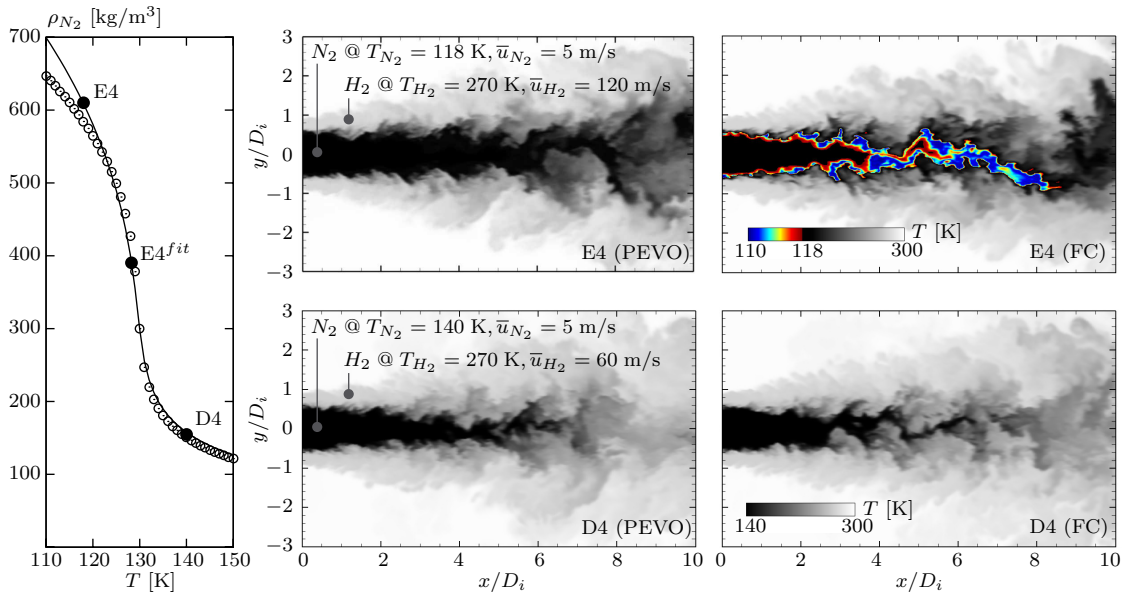

Figure 1: Left: Density prediction of the PR EOS (———) in comparison to the NIST reference data (⊙) (Linstrom & Mallard, 2015) for nitrogen at 4 MPa. Nitrogen injection conditions for case E4 (118 K), E4^{fit} (128.274 K) and D4 (140 K) are indicated by (●). Right: Instantaneous snapshots of the temperature distribution for the cases E4 and D4, each case simulated with the governing equations in fully conservative form (FC) and with the pressure evolution equation (PEVO).

tor for the FC approach $\phi^{FC} = [\rho, \rho u_k, E, \rho Y_i]^T$ consists of density ρ, momentum ρu_k, total energy $E = \rho e + \frac{1}{2}\rho u_k u_k$ (i.e., internal energy, e, plus kinetic energy), and partial density ρY_i of species i. $\mathbf{u} = [u_1, u_2, u_3]^T$ is the velocity vector in a Cartesian frame of reference. For the QC formulation, the total energy is replaced by the pressure p, i.e. $\phi^{QC} = [\rho, \rho u_k, p, \rho Y_i]^T$.

$$\partial_t \rho + \nabla\cdot(\rho\mathbf{u}) = 0 \tag{1}$$

$$\partial_t \rho\mathbf{u} + \nabla\cdot(\rho\mathbf{u}\cdot\mathbf{u}^\top + \mathbf{I}p) = \nabla\cdot\tau \tag{2}$$

$$\partial_t \rho Y_i + \nabla\cdot(\rho Y_i\mathbf{u}) = \nabla\cdot\mathbf{J}_i \tag{3}$$

$$\partial_t E + \nabla\cdot[(E+p)\mathbf{u}] = \nabla\cdot(\tau\cdot\mathbf{u} - \mathbf{q}) \tag{4}$$

$$\partial_t p + \nabla\cdot(p\mathbf{u}) = (p-\rho c^2)\nabla\cdot\mathbf{u} + \frac{\alpha_p}{c_v\beta_T\rho}\left[\nabla\cdot(\tau\cdot\mathbf{u}-\mathbf{q}) - \mathbf{u}\cdot(\nabla\cdot\tau)\right] + \sum_{i=1}^{N}\frac{1}{\rho}\frac{\partial p}{\partial Y_i}\bigg|_{\rho,e,Y_j[i]}\nabla\cdot\mathbf{J}_i \tag{5}$$

According to the Stokes hypothesis for a Newtonian fluid, the viscous stress tensor is

$$\tau = \mu\left(\nabla\mathbf{u} + (\nabla\mathbf{u})^T - 2/3\,\mathbf{I}\,\nabla\cdot\mathbf{u}\right), \tag{6}$$

with μ being the dynamic viscosity and $\mathbf{I}$ the unit tensor. The diffusional fluxes are calculated via the Fickian diffusion approximation that is

$$\mathbf{J}_i = \rho\left(D_i\nabla Y_i - Y_i\sum_{j=1}^{N} D_j\nabla Y_j\right) \tag{7}$$

where

$$D_i = (1-x_i)\left(\sum_{j\neq i}^{N}\frac{x_j}{D_{ij}}\right)^{-1} \tag{8}$$

is an effective binary diffusion coefficient for the diffusion

Table 1: Test case definition.

	p [MPa]	T_{N_2}	$\overline{u}_{N_2}$ [m/s]	ρ_{N_2} [kg/m^3]	$\dot{m}_{N_2}$ [g/s]	T_{H_2}	$\overline{u}_{H_2}$ [m/s]	ρ_{N_2} [kg/m^3]	$\dot{m}_{H_2}$ [g/s]
D4	4[a]	140[a]	5[a]	150.70[b] / 157.84[c]	2.14[b]/2.24[c]	270[a]	60[a]	3.50[b]/ 3.55[c]	0.96[b]/0.97[c]
E4	4[a]	118[a]	5[a]	584.43[b] / 608.78[c]	8.29[b]/8.63[c]	270[a]	120[a]	3.50[b]/ 3.55[c]	1.92[b]/1.94[c]
E4^{fit}	4	128.274	7.49	390.18	8.29	270	120	3.55	1.94

[a] Nominal experimental operating conditions according to Oschwald *et al.* (1999). [b] Calculated using NIST. [c] Calculated using the PR EOS. [d] Mass flow and density fitted boundary condition with $\dot{m}_{N_2}$ = 8.29 g/s and ρ_{N_2} = 390.18 kg/m^3, cf. Fig. 1.

of species i into the rest of the mixture, c.f. Cook (2009) and references therein. x_i denotes the mole fraction of species i. The physical binary mass diffusion coefficients D_{ij} are modeled according to Chapman and Enskog theory (see e.g. Prausnitz *et al.*, 1998). The vector

$$\mathbf{q} = -\kappa \nabla T - \sum_{i=1}^{N} h_i \mathbf{J}_i \tag{9}$$

consists of the conductive heat flux described by Fourier law and the interdiffusional enthalpy flux where κ is the thermal conductivity, T is the temperature, and h_i is the partial massic enthalpy of species i. Viscosity and thermal conductivity are described with the correlation of Chung *et al.* (1988) (note that the acentric factor of hydrogen was set to zero for the viscosity and thermal conductivity calculation since we observed a singularity in the correlation of Chung for the binary H_2/N_2 mixture).

In Eq. (5), c denotes the speed of sound, c_v is the heat capacity at constant volume, and α_p and β_T are the thermal expansion and isothermal compressibility coefficient, respectively. While Terashima & Koshi (2012) neglect the effect of a molecular diffusion induced pressure variation we take its contribution into account. It is worth noting that the implementation of Eq. (5) into an existing density based LES solver with explicit time integration is straightforward.

Equation (1)-(4) **or** (1)-(3) and (5) are closed by a cubic equation of state (CEOS) which can be universally expressed in their pressure explicit form, (cf. Kim *et al.*, 2012)

$$p(\underline{v}, T, x_1 \ldots x_N) = \frac{\mathcal{R}T}{\underline{v} - b} - \frac{a\alpha(T)}{\underline{v}^2 + ub\underline{v} + wb^2} \tag{10}$$

with the pressure p being a function of the specific molar volume $\underline{v}$, temperature T and the mole fractions x_1 through x_N. The model constants (u, w) take the values $(2, -1)$ for the Peng-Robinson (PR) EOS, which is used for the present simulations. The α-function in the attractive term is a correlation of temperature T, critical temperature T_c and acentric factor ω. The parameter a includes attractive forces between molecules, the effective molecular volume is represented by the parameter b. For the calculation of the coefficients $a\alpha(T)$ and b for a mixture composed of an arbitrary number of components we follow the recommendations given by Harstad *et al.* (1997) for which off-diagonal elements are calculated using the same expression as for the diagonals together with pseudo-critical parameters.

The governing equations of the FC formulation, Eq. (1)-(4), are discretized by a conservative finite-volume scheme on a Cartesian grid. In order to avoid spurious oscillations at sharp density gradients, we use a second-order upwind biased numerical flux function together with the van Albada limiter (van Albada *et al.*, 1982) for the advective transport of mass and internal energy. Effects of unresolved subgrid scales (SGS) are modelled by the adaptive local deconvolution method (ALDM) of Hickel *et al.* (2014), leading to a formulation in which only the compressible modes are affected by the second-order upwind scheme, while vorticity modes and turbulence kinetic energy remain unaffected. The viscous flux is discretised using a 2^{nd} order central difference scheme, and the 3^{rd} order explicit Runge-Kutta scheme of Gottlieb & Shu (1998) is used for time integration. The left hand side of the pressure advection equation is discretized consistently with the internal energy transport, such that both methods are numerically identical for a single-species perfect gas.

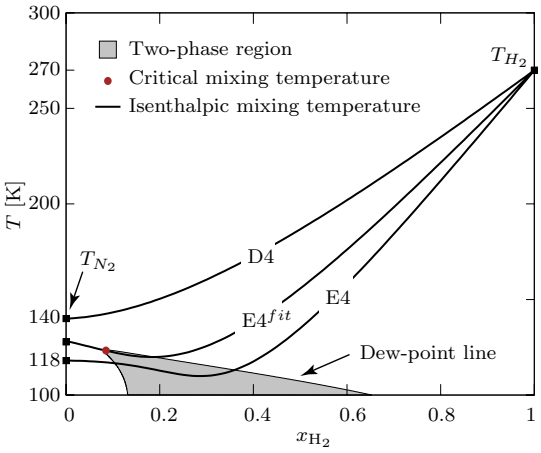

Figure 2: Binary phase diagram for a H_2 (right) N_2 (left) mixture as a result of a vapor-liquid equilibrium (VLE) calculation with the PR EOS. Solid lines labeled as D4, E4 and $E4^{fit}$ correspond to the adiabatic mixture temperature for a H_2/N_2 system at 4 MPa.

Experimental Setup

To be suitable for the validation of physical models or numerical methods benchmark experiments should have reduced complexity to validate individual processes and well defined boundary conditions. In this context, Oschwald *et al.* (1999) performed an experiment with particular emphasis on atomisation and mixing mechanisms for a single coaxial injector element operating under supercritical pressures (with respect to the critical pressure of the pure nitrogen). We confine our study to two selected operating conditions, E4 and D4, for which the experimental boundary conditions are summarized in Tab 1. Hydrogen (outer) and nitrogen (inner) are injected through a coaxial injector element into a cylindrical tank (D = 10 cm) filled with nitrogen at 4 MPa and 298.15 K. The inner and outer diameter of the hydrogen annulus are $D_{H_2,i}$ = 2.4 mm and $D_{H_2,o}$ = 3.4 mm, respectively, the inner nitrogen injector is 1.9 mm in diameter (D_i). Figure 1 (left) illustrates the two nominal operating conditions for the main nitrogen injection by means of a (ρ, T) diagram. While nitrogen is initially in a transcritical state for test case E4 (T_{N_2} = 118 K, liquid-like, left of the *Widom-line* (see Banuti, 2015)), it is supercritical for test case D4 (T_{N_2} = 140 K, gas-like, right of the *Widom-line*). Note that the temperature difference of only 22 K leads to a large density difference of 584.43 kg/m^3 and 150.70 kg/m^3 for the cases E4 and D4, respectively. As seen from Fig. 1 (left), the PR EOS yields a good approximation of the nitrogen inflow density for the selected nominal operating conditions in comparison to the NIST reference data ($\sim$ 4% error for case E4). Besides the differences related to the nominal thermodynamic state of pure nitrogen at injection, the cases E4 and D4 differ additionally in thermodynamic aspects that are associated to the binary mixing of nitrogen and hydrogen. Consider Fig. 2 showing a binary phase diagram for a H_2/N_2 mixture from a vapor-liquid equilibrium (VLE) calculation (criterion: equal fugacity in both phases for each single component at a given temperature and pressure) with the PR EOS: In general, a binary system lying

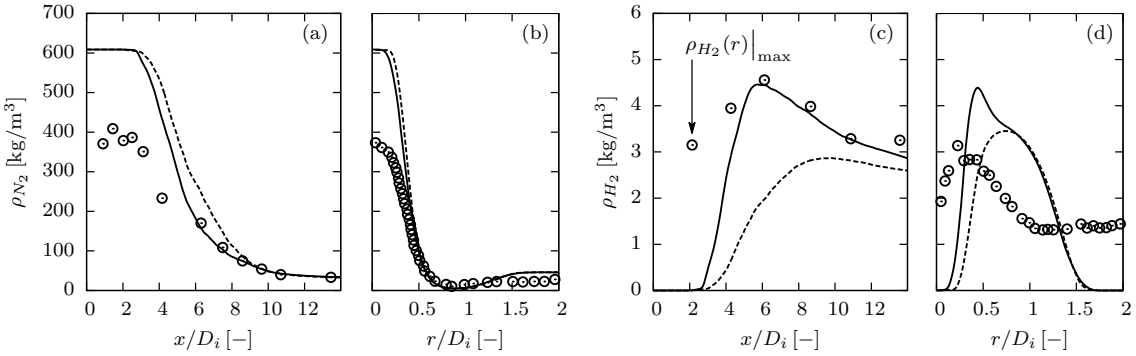

Figure 3: Axial (centerline) and radial nitrogen $\{\rho_{N_2}$, (a) and (b)$\}$ and hydrogen $\{\rho_{H_2}$, (c) and (d)$\}$ density profiles for test case E4. (———) Fully conservative (FC) method; (− − − −) Pressure evolution equation (PEVO); (⊙) Experimental data of Oschwald *et al.* (1999). Radial profiles are extracted at 4 mm. Note that 3 (c) displays numerical centerline data together with the experimentally observed maximal values of the radial hydrogen density distribution.

within the parameter space enclosed by the dew-point and bubble-point line (grey shaded region) is separated by an interface (of which properties are still to be determined) in a liquid and vapor phase. The solid lines labeled as D4 and E4, which partially intersect the two-phase region, depict the adiabatic mixture temperature of a H_2/N_2 system at 4 MPa. Note that for case E4 the adiabatic mixture temperature drops below 118 K, thus, showing the strongest real gas effects. From a thermodynamic perspective (and based on the assumption that the VLE calculation with the PR EOS and $k_{ij} = 0$ reproduces the mixture's real fluid behavior), phase separation, i.e. is the existence of a well-defined molecular interface, between the cryogenic N_2 and warm H_2 within the turbulent mixing layer may occur for the nominal experimental conditions of case E4. Recently, Dahms & Oefelein (2013) gave a very thorough discussion on the transition between two-phase and single-phase interface dynamics at supercritical pressures. Their results suggest that only a more in-depth analysis based on a Knudsen number criterion (i.e. molecular mean free path in the vapor phase over characteristic interface thickness) can answer the question whether a continuous gas like interface or a molecular vapor-liquid interface may exist for the experimental conditions of test case E4. In contrast, inflow and **all** adiabatic mixing temperatures of case D4 are well above the critical mixing temperature at 4 MPa, thus, the assumption holds of a continuous interfacial diffusion layer between the cold nitrogen and warm hydrogen. For details on the calculation of the VLE diagram it is referred to Jarczyk (2013) and Müller *et al.* (2015).

Grid and Boundary Conditions

All computations have been performed in a rectangular domain with the overall dimensions $L_x = 100$ mm in the streamwise and $L_y = L_z = 120$ mm in the lateral directions. The injector plane, 4 mm × 4 mm, is resolved with 16348 computational cells ($\Delta y_{min} = \Delta z_{min} = 0.03125$ mm). With increasing distance from the injector centerline ($y, z = \{\pm 2$ mm, ± 6 mm, ± 14 mm, ± 30 mm$\}$), a grid coarsening in spanwise directions by a factor of two is applied. For $x < 20$ mm and -6 mm $< y/z < 6$ mm the grid yields a homogenous streamwise resolution of $\Delta x_{min} = 0.078125$ mm. To ensure that jet dynamics are not affected by the subsonic outflow boundary condition, a hyperbolic grid stretching in streamwise direction is applied for $x > 20$mm. The total number of computational cells is $\approx 29 \cdot 10^6$. Realistic turbulent inflow data for the N_2 and H_2 jets are provided through a separate precursor incompressible LES using cyclic boundary conditions in axial direction. Slices of the turbulent velocity fields are extracted from this simulation, accumulated in a database and interpolated onto the coarser grid of the final coaxial jet simulation. Using the same transient inflow data for the FC and QC cases allows for the isolated assessment of the respective method. At the outlet we prescribe the static pressure of 4 MPa together with a linear extrapolation procedure of all conservative flow variables. All walls are modeled as adiabatic.

RESULTS AND DISCUSSION

Figure 1 (right) depicts a contour plot of the instantaneous temperature distribution for the cases E4 and D4, each simulated with the governing equations in FC form and with the PEVO. Contour levels are shown for 118 K $< T <$ 300 K, from dark to light shades, superimposed by a second group of contour levels with 110 K $< T <$ 118 K, from blue to red shades. While we observe qualitatively a remarkably good agreement between FC and QC formulation for case D4, some differences arise for case E4. As seen in Fig. 1, only in case of a FC formulation the temperature in the mixing layer drops below its inflow value of 118 K to approximately 110 K. This observation can be attributed exclusively to real gas mixing effects, cf. Fig. 2. Furthermore, it follows that the model assumption of an adiabatic and isobaric mixing process (as done for Fig. 2) yields a good approximation of the actual mixing process, see also Lacaze *et al.* (2015) and Müller *et al.* (2015).

In the following we compare our numerical results obtained with the FC formulation to the experimental data of Oschwald *et al.* (1999). Figure 3a and 3b depict the axial (centerline) and radial nitrogen density profiles for test case E4. We observe significant differences in the potential core region ($x/D_i < 3$) with an experimental and numerical nitrogen density of ~ 390.18 kg/m^3 and ~ 608.78 kg/m^3, respectively. Recall Fig. 1 (left): the definition of inflow boundary conditions in terms of temperature and pressure must yield a density prior jet break-up much higher than what is observed experimentally. Note that the observed differences in density of approximately ~ 200 kg/m^3 can not be

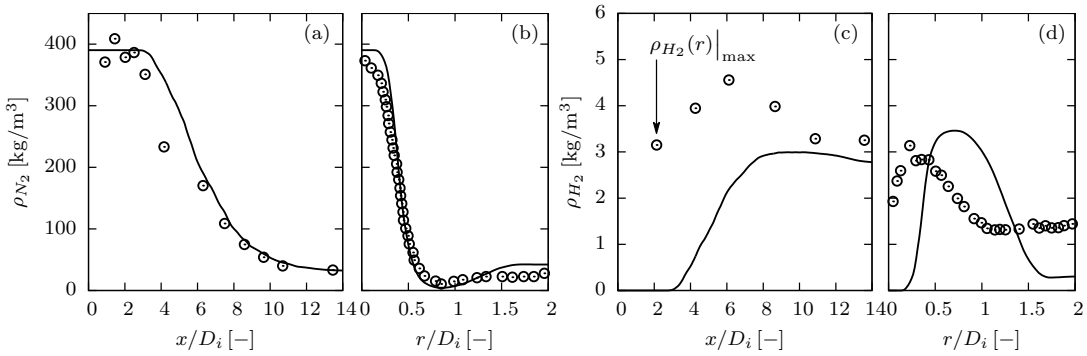

Figure 4: Axial (centerline) and radial nitrogen $\{\rho_{N_2}$, (a) and (b)$\}$ and hydrogen $\{\rho_{H_2}$, (c) and (d)$\}$ density profiles for test case E4^{fit}. (———) Fully conservative (FC) method; (⊙) Experimental data of Oschwald *et al.* (1999). Radial profiles are extracted at 4 mm. Note that 3c displays numerical centerline data together with the experimentally observed maximal values of the radial hydrogen density distribution.

attributed to an inaccurate equation of state, compare Tab. 1 and Fig. 1. Figure 3c and 3d depict the corresponding hydrogen density. Note that Fig. 3c displays numerical centerline data together with the experimentally observed maximal values of the radial hydrogen density distribution. Interestingly, Oschwald *et al.* (1999) report an increase in hydrogen density downstream of the jet break-up that exceeds its pure-component value at injection. From a phenomenological/qualitative perspective we are able to reproduce this effect in the numerical simulation, see Fig. 3c. Quantitatively, however, we obtain large deviations between measured and simulated hydrogen density. Note that the increase in hydrogen density is caused by real gas mixing effects rather than by a heat transfer and diffusion mechanism from the warm hydrogen to the cryogenic nitrogen.

Measurements in a high pressure low temperature environment are very demanding and introduce a number of uncertainties. Oschwald *et al.* (1999) report beam steering and reflection issues along with problems to determine the inlet temperature of the cryogenic nitrogen. Since the nitrogen density at injection is very sensitive to small changes in temperature, cf. Fig. 1 (left), we believe that the observed discrepancies between experiment and simulation may be founded in a different nitrogen temperature prior to injection. Assuming a correct density (390.18 kg/m^3) and mass flow rate (8.29 g/s) measurement (rather than temperature measurement), we define a test case E4^{fit} with a fitted nitrogen bulk velocity $\bar{u}_{N_2}$ = 7.49 m/s and inflow temperature T_{N_2} = 128.274 K. Figure 4a and 4b depict the corresponding centerline and radial nitrogen density profiles. We now observe a very good agreement for the absolute value of the predicted nitrogen density, the potential core length (i.e. location of break-up) and the axial position for which a fully mixed state is obtained ($x/D_i \sim 10$). We note that the location of jet break-up and downstream evolution ($\partial\rho/\partial x$) is very sensitive to the numerical scheme that is used, compare also our results documented in Müller *et al.* (2015). At a first glance, these results suggest that the nitrogen temperature at injector exit could have been higher at the time of data collection. However, we are now lacking the increase in hydrogen density downstream of the jet break-up that exceeds its pure component value at injection, see Fig. 4c and Fig. 4d.

As the preceding discussion has shown, there is a need for a broader quantitative experimental data base. To our knowledge, the only (published) quantitative data on inert coaxial injection at trans- and supercritical pressures are the data of Oschwald *et al.* (1999). Possible reasons for the observed differences between experiment and numerical simulation are manifold, and their interpretation can be ambiguous.

In the following we characterize the differences between the FC and QC formulation for test case E4: The location of jet break-up is shifted downstream for the QC formulation, see Fig 3a. This is consistent with the observation of a lower fluctuating pressure level $\langle p'p' \rangle$ (not shown here), which is expected to amplify jet break-up dynamics, and the design (satisfying velocity and pressure equilibrium at fluid interfaces) of this numerical method. The increase in hydrogen density downstream of the jet break-up is not reproduced by the QC formulation, see Fig 3c and 3d. We want to emphasize that the reasons for the observed differences between FC and QC formulation for test case E4 are currently not well understood and are subject of ongoing research. For the operating conditions of test case D4 we obtain a perfect match between FC and QC formulation, see Fig. 5.

CONCLUSIONS

The coaxial injection of cryogenic nitrogen and warm hydrogen into a supercritical nitrogen atmosphere was studied numerically by means of well resolved large-eddy simulation. We compared a fully conservative (FC) to a quasi conservative (QC) formulation of the governing equations for two operating conditions of a series of experiments of Oschwald *et al.* (1999). While we observe qualitatively and quantitatively a remarkably good agreement between FC and QC formulation at supercritical operating conditions (D4), some differences exist in case of transcritical nitrogen injection (E4): Flow features that are caused by real gas mixing effects / equation of state peculiarities, such as hydrogen densities downstream of the jet break-up that exceed its pure component value at injection, are not present in case of the QC form of the governing equations.

From a qualitative perspective, we were able to reproduce the characteristic increase in hydrogen density downstream of jet break-up that has been recorded experimentally for the nominal operating conditions of test case E4. Based on the observation that the definition of inflow boundary conditions in terms of temperature and pres-

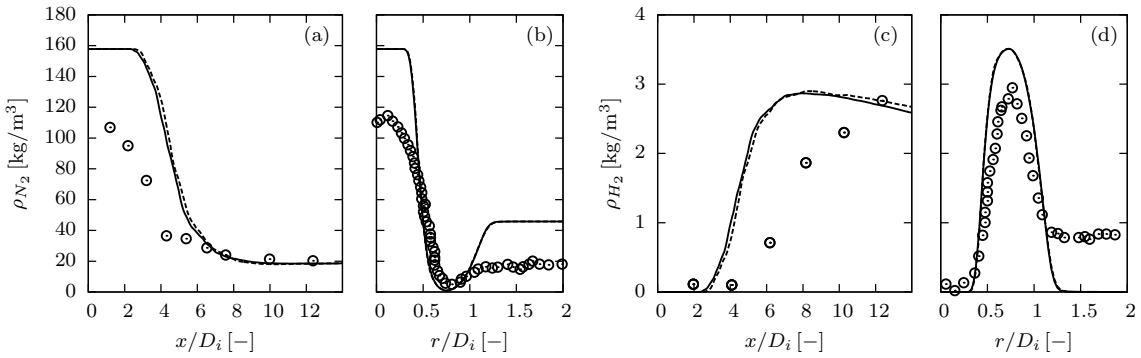

Figure 5: Axial (centerline) and radial nitrogen $\{\rho_{N_2}$, (a) and (b)$\}$ and hydrogen $\{\rho_{H_2}$, (c) and (d)$\}$ density profiles for test case D4. (———) Fully conservative (FC) method; (− − − −) Pressure evolution equation (PEVO); (⊙) Experimental data of Oschwald *et al.* (1999). Radial profiles are extracted at 2 mm.

sure must yield a density prior jet break-up much higher than what was measured experimentally, we defined a new test case for which bulk velocity and injection temperature are adjusted to match density and mass flow rate measurement (rather than temperature measurement). For this fitted boundary condition we observed a very good agreement between experimental and numerical data.

Acknowledgements

Financial support has been provided by the German Research Foundation (Deutsche Forschungsgemeinschaft DFG) in the framework of the SFB/TRR 40. Computational resources have been provided by the Leibniz Rechenzentrum München (LRZ).

REFERENCES

van Albada, G. D., van Leer, B. & Roberts Jr, W. W. 1982 A comparative study of computational methods in cosmic gas dynamics. *Astronomy and Astrophysics* **108**.

Banuti, D. T. 2015 Crossing the Widom-line – Supercritical pseudo-boiling. *The Journal of Supercritical Fluids* **98**.

Chehroudi, B., Talley, D. & Coy, E. 2002 Visual characteristics and initial growth rates of round cryogenic jets at subcritical and supercritical pressures. *Physics of Fluids (1994-present)* **14** (2).

Chung, T. H., Ajlan, M., Lee, L. L. & Starling, K. E. 1988 Generalized multiparameter correlation for nonpolar and polar fluid transport properties. *Industrial & Engineering Chemistry Research* **27** (4).

Cook, A. W. 2009 Enthalpy diffusion in multicomponent flows. *Physics of Fluids (1994-present)* **21** (5).

Dahms, R. N. & Oefelein, J. C. 2013 On the transition between two-phase and single-phase interface dynamics in multicomponent fluids at supercritical pressures. *Physics of Fluids (1994-present)* **25** (9).

Gottlieb, S. & Shu, C. 1998 Total variation diminishing Runge-Kutta schemes. *Mathematics of computation of the American Mathematical Society* **67** (221).

Harstad, K., Miller, R. S. & Bellan, J. 1997 Efficient high-pressure state equations. *AIChE Journal* **43** (6).

Hickel, S., Egerer, Christian P & Larsson, J. 2014 Subgrid-scale modeling for implicit large eddy simulation of compressible flows and shock-turbulence interaction. *Physics of Fluids (1994-present)* **26** (10).

Jarczyk, M. M. 2013 Numerische Modellierung von turbulenten Strömungen realer Gasgemische. PhD thesis, University of the Armed Forces, Munich, Germany.

Kim, S.-K., Choi, H.-S. & Kim, Y 2012 Thermodynamic modeling based on a generalized cubic equation of state for kerosene/LOx rocket combustion. *Combustion and flame* **159** (3).

Lacaze, G., Misdariis, Antony, Ruiz, Anthony & Oefelein, J. C. 2015 Analysis of high-pressure Diesel fuel injection processes using LES with real-fluid thermodynamics and transport. *Proceedings of the Combustion Institute* **35** (2).

Linstrom, P. J. & Mallard, W. G. 2015 *NIST Chemistry WebBook, NIST Standard Reference Database Number 69*. National Institute of Standards and Technology, Gaithersburg MD, 20899.

Masquelet, M., Guézennec, N. & Menon, S. 2012 Numerical Studies of Mixing and Flame-Turbulence Interactions in Shear Coaxial Injector Flows Under Trans-Critical Conditions. In *50th AIAA Aerospace Sciences Meeting including the New Horizons Forum and Aerospace Exposition*.

Mayer, W. O. H., Schik, A. H., Vielle, B., Chauveau, C., Gökalb, I., Talley, D. G. & Woodward, R. D. 1998 Atomization and breakup of cryogenic propellants under high-pressure subcritical and supercritical conditions. *Journal of Propulsion and Power* **14** (5).

Müller, H, Pfitzner, M., Matheis, J. & Hickel, S. 2015 Large-Eddy Simulation of Coaxial LN2/GH2 Injection at Trans-and Supercritical Conditions. In *53rd AIAA Aerospace Sciences Meeting*.

Oschwald, M., Schik, A., Klar, M. & Mayer, W. 1999 Investigation of Coaxial LN2/GH2-Injection at Supercritical Pressure by Spontaneous Raman Scattering . In *35th AIAA/ASME/SAE/ASEE Joint Propulsion Conference and Exhibit 20-24 June 1999 Los Angeles, California*.

Prausnitz, J. M., Lichtenthaler, R. N. & de Azevedo, E. G. 1998 *Molecular Thermodynamics of Fluid-Phase Equilibria*. Pearson Education.

Terashima, H. & Koshi, M. 2012 Approach for simulating gas–liquid-like flows under supercritical pressures using a high-order central differencing scheme. *Journal of Computational Physics* **231** (20).

Terashima, H. & Koshi, M. 2014 Numerical study on mixing characteristics of coaxial cryogenic N2/H2 injection under supercritical pressure. In *52nd Aerospace Sciences Meeting (AIAA)*.